



COMPUTER SIMULATION OF TOPOLOGICAL EVOLUTION IN 2-D GRAIN GROWTH USING A CONTINUUM DIFFUSE-INTERFACE FIELD MODEL

DANAN FAN, CHENGWEI GENG and LONG-QING CHEN

Department of Materials Science and Engineering, The Pennsylvania State University, University Park,
PA 16802, U.S.A.

(Received 30 January 1996; accepted 12 June 1996)

Abstract—The local kinetics and topological phenomena during normal grain growth were studied in two dimensions by computer simulations employing a continuum diffuse-interface field model. The relationships between topological class and individual grain growth kinetics were examined, and compared with results obtained previously from analytical theories, experimental results and Monte Carlo simulations. It was shown that both the grain-size and grain-shape (side) distributions are time-invariant and the linear relationship between the mean radii of individual grains and topological class n was reproduced. The moments of the shape distribution were determined, and the differences among the data from soap froth, Potts model and the present simulation were discussed. In the limit when the grain size goes to zero, the average number of grain edges per grain is shown to be between 4 and 5, implying the direct vanishing of 4- and 5-sided grains, which seems to be consistent with recent experimental observations on thin films. Based on the simulation results, the conditions for the applicability of the familiar Mullins–Von Neumann law and the Hillert's equation were discussed. Copyright © 1997 Acta Metallurgica Inc.

1. INTRODUCTION

The fundamental features of normal grain growth have been investigated extensively because of the importance of the microstructure in controlling the physical and mechanical properties of a polycrystalline material. During normal grain growth, the average grain size increases, driven by the reduction in the total grain boundary energy, and dynamical and topological interactions occur among individual grains.

Since the 1950s, many theories have been proposed to predict the time dependence of average grain size and size distributions [1–10]. In addition, the relationship between the topological requirements for space filling and the time dependence of average grain size has become one of the most studied subjects in normal grain growth [11–23].

Because of the complexity of topological interactions during grain growth, it is extremely difficult to describe the kinetics of grain growth and topological interactions between grains within a single analytical model. Therefore, computer simulations are playing a very important role in exploring the details of grain growth and testing the validity of analytical theories. For modelling grain growth, many approaches have been proposed, such as the statistical models [24–26], vortex models [27, 28], boundary dynamics models [29, 30], mean field theories [31–33], Voronoi models [34, 35] and the Potts model [36–39]. In spite of the different physical bases and approaches employed in these models, a

common feature is that the boundaries or interfaces are treated as having zero thickness in these models, i.e. as sharp interfaces. Very recently, we developed a continuum diffuse-interface model for studying the coarsening kinetics in single-phase and multi-phase materials [23, 40–42], in which the grain boundaries and interphase boundaries are treated as diffuse interfaces of finite thickness. One of the main features of the diffuse-interface model is the fact that one does not have to explicitly track the positions of grain boundaries since their locations are implicitly defined by the regions where the gradients of field variables are significant. Since the interfaces are diffuse, the lattice anisotropy effect can be kept to a minimum. Finally, in the diffuse-interface field model, it is straightforward to describe long-range diffusion, which takes place, for example, during solute segregation and second-phase precipitation at grain boundaries in a polycrystalline material, by coupling the kinetic equations for the orientation field variables with the Cahn–Hilliard non-linear diffusion equation for composition [43].

In previous papers [23, 40], using the diffuse-interface field model, we have shown that the average grain size of a pure system evolves following the growth law $R_t^m - R_0^m = kt$ with $m = 2$ in the scaling regime, which is independent of the number of field variables. A simulated microstructure evolution of grain growth is shown in Fig. 1. The size distribution function plotted against $\log(\bar{R}/R)$ has asymmetric characteristics and is self-similar or time-invariant.

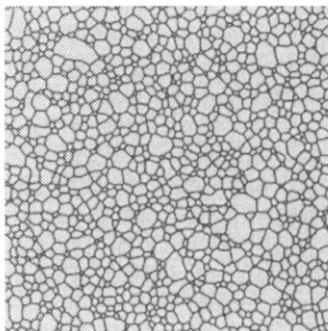
We also showed [23] that a log-normal distribution function fits into simulation data better near the average grain size region; however, it departs from simulation for small grains and large grains. Louat's distribution function agrees well with simulation results for large and small grains; however, it predicts a lower distribution peak near the average size region [23].

In this paper, we focus on the local kinetics for individual grains, especially, the relationship between the topological requirements and the growth kinetics using the continuum diffuse-interface model, and compare them with the predictions of analytical theories and results obtained from other computer simulations. In particular, the growth rates of individual grains, the dependence of the growth rates on the topological classes, the grain size distributions, as well as the interrelationships between these properties, are studied, based on the temporal evolution of microstructures generated from the computer simulations.

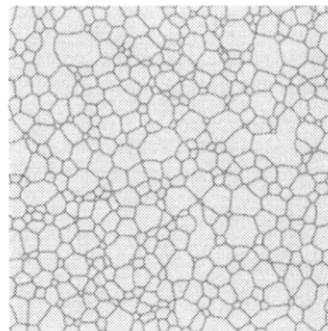
2. DIFFUSE-INTERFACE MODEL FOR GRAIN GROWTH

In the diffuse-interface field model [23, 40], an arbitrary polycrystalline microstructure is described by a set of continuous field variables,

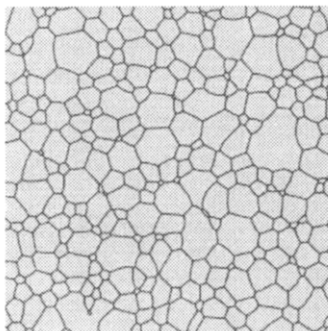
$$\eta_1(r), \eta_2(r), \dots, \eta_p(r)$$



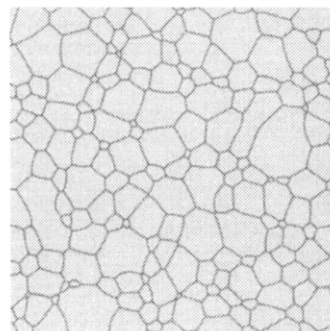
t=1000



t=3000



t=5000



t=8000

Fig. 1. Simulated microstructure evolution in 512×512 system with 36 orientation variables.

where p is the number of possible orientations in space and η_i ($i = 1, \dots, p$) are called orientation field variables which distinguish the different orientations of grains and are continuous in space. Their values continuously vary from -1.0 to 1.0 . In real materials, the number of orientations is infinite ($p = \infty$). However, it was shown that a finite number for p might be sufficient to realistically simulate grain growth [23].

Within the diffuse-interface theory [44], the total free energy of an inhomogeneous system can be written as

$$F = \iint \left[f_0(\eta_1(r), \eta_2(r), \dots, \eta_p(r)) + \sum_{i=1}^p \frac{\kappa_i}{2} (\nabla \eta_i(r))^2 \right] d^3r \quad (1)$$

where f_0 is the local free energy density which is a function of field variables η_i , and κ_i are the gradient energy coefficients. The origin of the grain boundary energy comes from the gradient energy terms $(\nabla \eta_i)^2$ in equation (1). The smaller the gradient energy coefficient κ_i , the thinner the boundary region. If all the gradient energy coefficients go to zero, the boundary thickness becomes infinitely thin, i.e. it becomes a sharp interface.

The spatial and temporal evolution of orientation field variables is described by the Ginzburg–Landau equations,

$$\frac{d\eta_i(r, t)}{dt} = -L_i \frac{\delta F}{\delta \eta_i(r, t)} = -L_i \left(\frac{\partial f_o}{\partial \eta_i} - \kappa_i \nabla^2 \eta_i \right),$$

$$i = 1, 2, \dots, p \quad (2)$$

where L_i are the kinetic coefficients related to grain boundary mobility, t is time and F is the total energy given in equation (1).

To simulate grain growth kinetics, we assumed the following simple free energy density functional

$$f_o(\eta_1, \eta_2, \dots, \eta_p)$$

$$= \sum_{i=1}^p \left(-\frac{\alpha}{2} \eta_i^2 + \frac{\beta}{4} \eta_i^4 \right) + \gamma \sum_{i=1}^p \sum_{j \neq i}^p \eta_i^2 \eta_j^2 \quad (3)$$

where α , β and γ are phenomenological parameters. The main requirement for f_o in modelling grain growth in a pure single phase is that it has p degenerate minima with equal depth, f_{\min} , located at $(\eta_1, \eta_2, \dots, \eta_p) = (1, 0, \dots, 0), (0, 1, \dots, 0), \dots, (0, 0, \dots, 1)$ in p -dimensional space. It can be shown that, if $\gamma > \beta/2$, equation (3) gives $2p$ potential minima (wells) in the p -field space, which represent the equilibrium free energies of crystalline grains in $2p$ different orientations.

3. NUMERICAL SIMULATION PROCEDURE

In the computer simulation, equations (2) are discretized in space and time. The Laplacian is discretized by the following equation:

$$\nabla^2 \eta_i = \frac{1}{(\Delta x)^2} \left[\frac{1}{2} \sum_j (\eta_j - \eta_i) + \frac{1}{4} \sum_k (\eta_k - \eta_i) \right] \quad (4)$$

where Δx is the grid size, j represents the first-nearest neighbours of site i , and k represents the second-nearest neighbours of site i . For discretization with respect to time, the explicit Euler equation is used:

$$\eta_i(t + \Delta t) = \eta_i(t) + \frac{d\eta_i}{dt} \times \Delta t \quad (5)$$

where Δt is the time step for integration.

In this paper, we employed 512×512 square lattice points to spatially discretize the kinetic equations with periodic boundary conditions applied along both Cartesian coordinate axes. The discretizing grid size Δx is chosen to be 2.0 and the time step Δt is 0.25. The number of orientations, p , is assumed to be 36, which is shown to provide a realistic simulation of microstructural evolution and growth kinetics [23]. For the local free energy density function, the following parameters were assumed: $\alpha = 1.0$, $\beta = 1.0$ and $\gamma = 1.0$; κ_i and L_i were chosen to be 2.0 and 1.0 for all orientations and give an

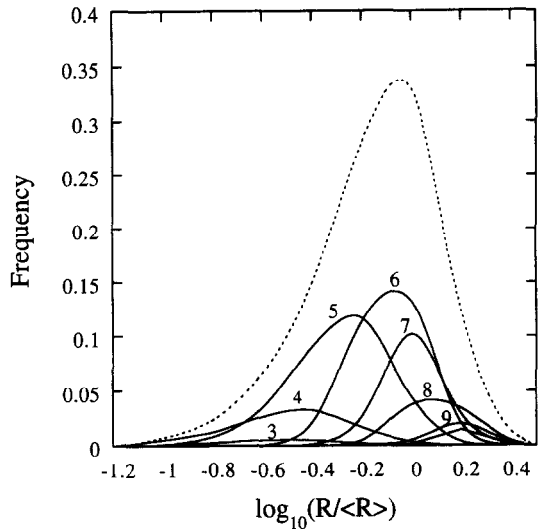


Fig. 2. Grain size distributions according to topological class (numbers in figure) of grains. The dashed line is the overall grain size distribution.

isotropic grain boundary energy and isotropic grain boundary mobility, respectively. The computer simulations started from a liquid phase by assigning small random values, e.g. between -0.001 and 0.001 , to all orientation variables at all grid points, and then allowing crystallization to occur, which generates a fine grain microstructure. The crystallization is finished after about 200 time steps. Allowing sufficient time for the system to reach the scaling state, e.g. 1000 time steps, individual grains were monitored for calculating their growth rates, the topological distributions and other topological and kinetic information. At time step 1000, there are more than 1200 grains in the system. The area of a grain, A , at a certain time step, is directly obtained from the microstructure by summing the number of grid points within the grain, and the grain radius, R , is calculated from the area through $A = \pi R^2$ as an approximation. The average grain size at a certain time is obtained by averaging the grain size over all grains in the system. The growth rates of individual grains, dA/dt and dR/dt , were calculated according to $dA/dt = [A(t + \Delta t) - A(t)]/\Delta t$ or $dR/dt = [R(t + \Delta t) - R(t)]/\Delta t$, every 1000 time steps with Δt equal to 20 time steps. All the kinetics data presented were obtained by averaging over several independent simulation runs in an attempt to get better statistics.

4. SIMULATION RESULTS

4.1. Static properties and topology

The first property studied is the dependence of the size distribution function $\rho(R)$ on topological class. The frequency of grain occurrence as a function of grain size in different topological classes, obtained from the microstructure at time step 1000, is shown in Fig. 2 in which the dashed line represents the size distribution function for all the grains and the solid

lines are the size distributions for grains in a given topological class. It can be seen that the peak height of the size distribution for a given topological class increases as the number of grain sides increases from 3 to 6, and then decreases when the topological class is larger than 6, whereas the width of the size distributions decreases as the number of grain sides increases. It is quite clear from Fig. 2 that the peak of the overall size distribution for all grains comes mainly from the contributions of 5-, 6- and 7-sided grains. As expected, few-sided grains tend to have smaller sizes while many-sided grains are more likely to have larger sizes. Moreover, smaller-sided grains seem to have much wider size distributions.

To investigate the relationship between the grain-shape distribution and topological classes, the frequency of occurrence of grains with a certain number of sides is plotted against the number of sides n at several selected time steps in Fig. 3. It appears that the shapes of the distribution $\rho(n)$, similar to the size distribution function $\rho(R)$, are self-similar at different time steps, i.e. it is time-invariant. It is also observed that 5-sided grains have the highest frequency of occurrence at all times and 6-sided grains are the second highest. However, the average number of grain sides over all grains in the system is very close to 6 at all times as shown in Fig. 4, which satisfies the requirement of space filling. The average number of sides over time \bar{n} obtained from Fig. 4 is 5.995.

Another property calculated is the moment of the grain side distribution, which is defined as:

$$\mu_m = \sum_{n=2}^{\infty} \rho(n)(n - \langle n \rangle)^m \quad (6)$$

where μ_m is the m th moment of the side distribution function $\rho(n)$ and $\langle n \rangle$ the average number of grain sides at a certain time. The moment of the side

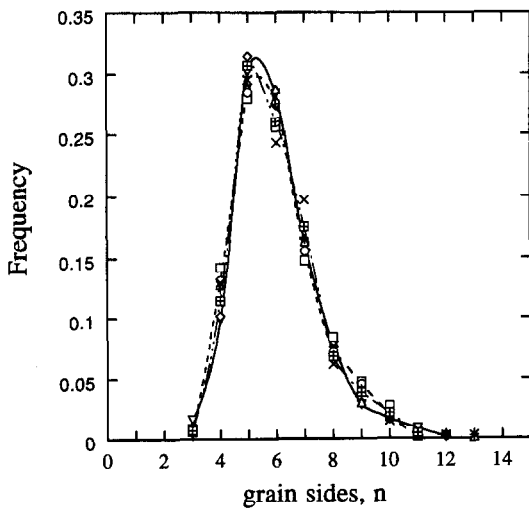


Fig. 3. Grain edge distributions at different time steps. In the scaling region, the shape of the grain edge distribution is time-invariant.

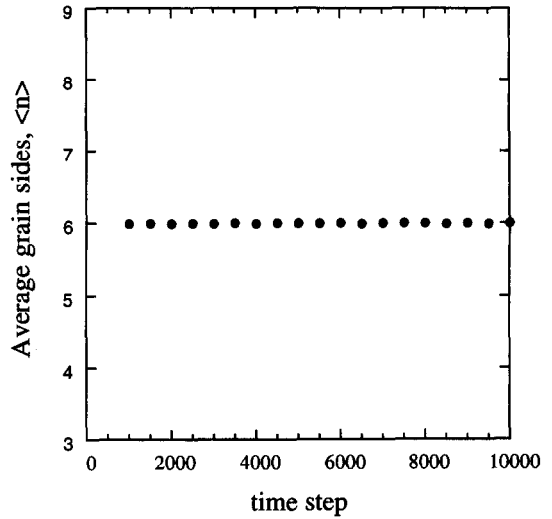


Fig. 4. Average number of grain sides of all grains at different time steps.

distribution is an important indicator of the topological characteristics of a system during grain growth. Moments larger than μ_2 are much more sensitive to the large- n tail of the side distribution and to the measurement error, and hence, normally they are only useful for qualitative analysis. The time dependence of the second moment of the side distribution μ_2 is shown in Fig. 5. It can be seen that, after the initial 1000 time steps, the values of μ_2 are almost constant as a function of time with a small fluctuation, which indicates that the system has reached the scaling state and good statistics were obtained for calculating the side distribution. The average value for μ_2 is 2.33 ± 0.13 , which is very close to the Monte Carlo simulation result $\mu_2 = 2.49$ [39].

The correlation function between the number of sides n of a grain and the average sides of its

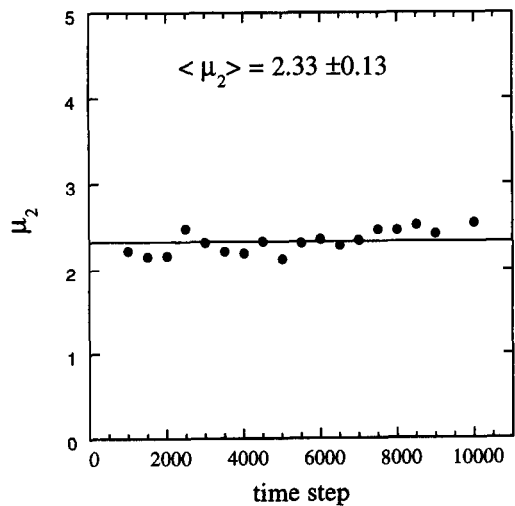


Fig. 5. Time dependence of second moment μ_2 of grain edge distribution. The solid line is the average value of μ_2 , $\langle \mu_2 \rangle = 2.33 \pm 0.13$.

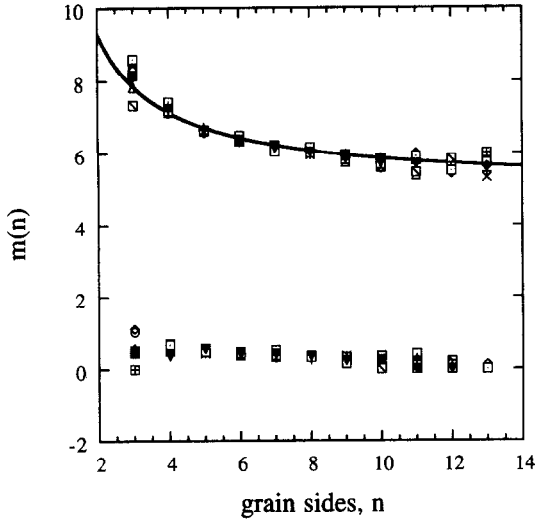


Fig. 6. Neighbour side correlation function $m(n)$ and its standard deviation at ten different time steps. The solid line is the data fitted into equation (11) with $a = 1.0$ and $\mu_2 = 2.34$.

neighbours, $m(n)$, as defined by Aboav [45], has a form

$$m(n) = 5 + \frac{8}{n}. \tag{7}$$

A more general form, as suggested by Weaire [46], is

$$m(n) = 6 - a + \frac{6a + \mu_2}{n}, \tag{8}$$

where μ_2 is the second moment of the side distribution and a is a constant with its value close to unity. This equation is called the Aboav–Weaire law. The $m(n)$ values and their standard deviations calculated at different time steps from our simulation data are shown in Fig. 6. It can be seen that few-sided grains tend to have many-sided grains as neighbours whereas the average number of sides for neighbouring grains around a many-sided grain is close to 6. It is observed that the correlation function $m(n)$ is time-invariant in the scaling region and the average values of $m(n)$ have an excellent fit to equation (8). The solid line in Fig. 6 is the fit of equation (8) with $a = 1.0$ and $\mu_2 = 2.57$. On the other hand, if the average data is fitted to equation (8) with two free parameters a and μ_2 , the best fit is $a = 1.28$ and $\mu_2 = 2.34$. It may be noted that the two curves generated by $a = 1.0$ and $\mu_2 = 2.57$, and by $a = 1.28$ and $\mu_2 = 2.34$ do not have significant differences. This result seems to agree with the Monte Carlo Potts model simulation [39].

Lewis [6] showed that, for two-dimensional polygonal cells, the average area of an n -sided polygonal cell is a linear function of the cell sides n :

$$\langle A_n \rangle = \beta(n - n_0), \tag{9}$$

where $\langle A_n \rangle$ is the average area of n -sided cells at a given time, β and n_0 are constants dependent on the properties of the structure. This relationship is true at

any fixed time. The results extracted from our simulation data are presented in Fig. 7. In Fig. 7, the average area of n -sided grains was normalized by the average area of total grains at that time step for comparing the results from different times. It can be seen that results obtained from different time steps agree with each other reasonably well within statistical errors. However, the linear relationship given by equation (9) seems to be followed only for intermediate topological classes. By averaging the data over different time steps and independent runs, it is found that for 3- and 4-sided grains the Lewis law predicts negative areas if the data were fitted to equation (9), i.e. few-sided grains have a larger area than the Lewis' law predicted. For grains with 5–10 sides, the linear relationship between average areas and grain sides n is held reasonably well, whereas the average areas for many-sided grains ($n > 12$) are, again, larger than those predicted by equation (9).

On the other hand, Feltham [4], based on a study of three-dimensional grain growth, predicted a linear relationship between the average grain radius of n -sided grains and the topological classes n , i.e.

$$\langle R_n \rangle = \beta'(n - n'_0) \tag{10}$$

where β' and n'_0 are constants. This relationship is tested in Fig. 8 by plotting normalized grain radius $R_n/\langle R \rangle$ as a function of topological class n for different time steps. A very good linear relationship is observed for all times. Averaging data over different runs and different time steps yields an excellent linear dependence of average radius of n -sides grains on the topological class n .

4.2. The kinetics of individual grains

One of the advantages of computer simulations is that the properties of a large number of individual

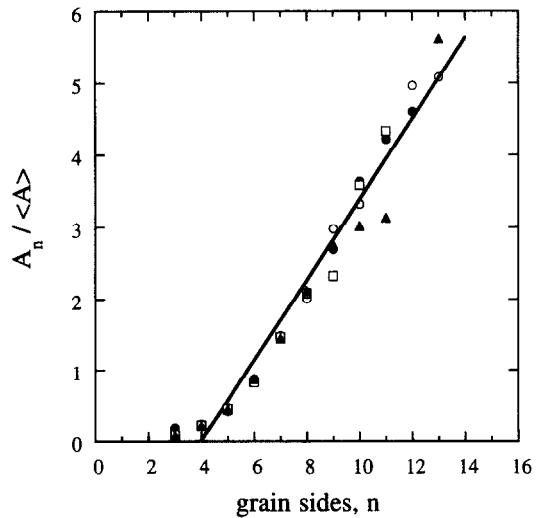


Fig. 7. Relationship between normalized average grain area $\langle A_n \rangle / \langle A \rangle$ and topological class n at different time steps. The solid line is the linear fit to the average data from different times.

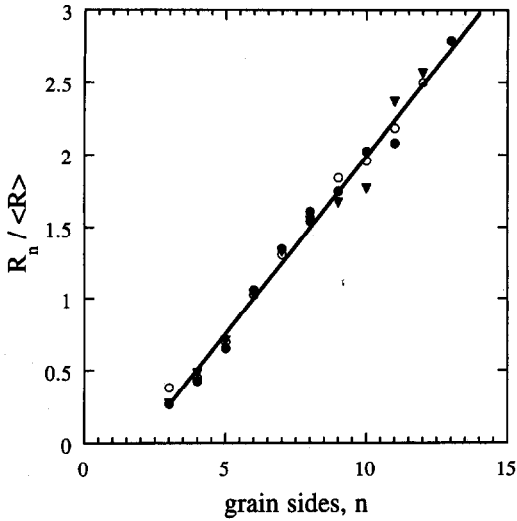


Fig. 8. Relationship between normalized average grain radius $\langle R_n \rangle / \langle R \rangle$ and topological class n at different time steps. The solid line is the linear fit to the average data from different times.

grains can be monitored and hence the assumptions or relationships proposed by analytical theories can be examined. The Mullins–Von Neumann law requires a linear relationship between the growth rates of individual grains and their topological classes:

$$\frac{dA}{dt} = \frac{\pi M \sigma}{3} (n - 6) \quad (11)$$

where M is the grain boundary mobility and σ is the grain boundary energy. This relationship was quantitatively examined by monitoring the growth rates of individual grains for different topological classes at various times. Figure 9 is a plot of

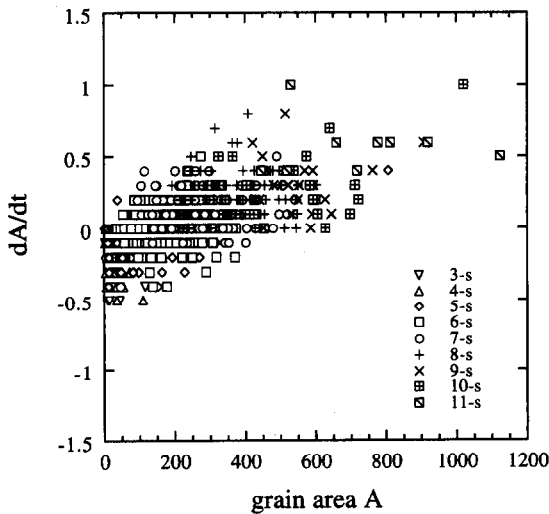


Fig. 9. Dependence of growth rate dA/dt on grain area A and topological class n for individual grains at time step $t = 1000$. In the figure, 3s means 3-sided grains, 4-s 4-sided grains, and so on.

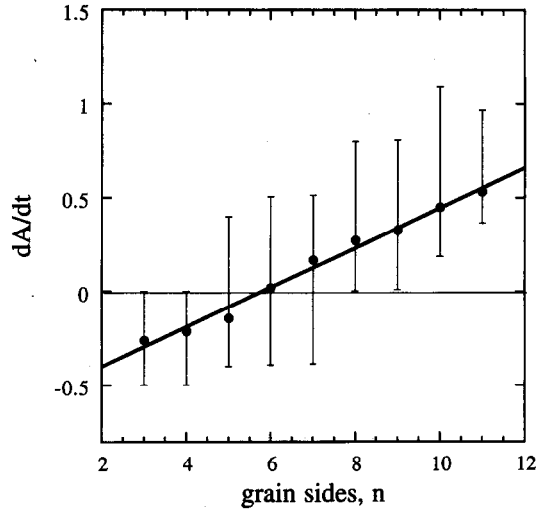


Fig. 10. Relationship between average growth rate dA/dt and topological class n for about 4000 grains. The solid dots are the average growth rates in each topological class and the solid line is a linear fit to equation (11). The error bars represent the maximum and minimum growth rates observed in each topological class.

individual growth rates dA/dt against the grain area A for different topological classes at a time step of 1000, by examining more than 1200 grains. It can be seen that although most of the large grains have many sides and a positive growth rate ($dA/dt > 0$), this is not always true. For example, many small grains with 7 sides have negative growth rates ($dA/dt < 0$), i.e. some 7-sided grains shrink instead of growing. It is also common that many-sided grains have a zero growth rate ($dA/dt = 0$) within certain time intervals. Similarly, although the majority of small grains have fewer sides than 6 and have negative growth rates, some 5-sided grains may have significantly larger size and actually grow. For 6-sided grains, their sizes are more concentrated at the average grain size, and both growth and shrinkage of 6-sided grains are observed even though most of them have a zero growth rate.

The average growth rates of individual grains for about 4000 grains are plotted in Fig. 10 according to the topological class. In the plot, the solid dots are the average growth rates in each topological class and the solid line is a linear fitting to equation (11). The error bars represent the maximum and minimum growth rates observed in each topological class. It is clear that many-sided grains ($n > 8$) tend to grow and few-sided grains ($n < 5$) tend to shrink. However, situations are much more complicated for 5-, 6- and 7-sided grains. Those grains can either grow or shrink as well as have zero growth rate depending on their sizes and their neighbour grains or local topology arrangements. The difference is that the majority of 5-sided grains shrink and most 7-sided grains grow while most of the 6-sided grains have a zero growth rate. As a result, the average growth rate for 5-sided grains is negative, that for 7-sided grains is positive and as expected it is zero for 6-sided grains. It can be

seen that the Mullins–Von Neumann law is obeyed [equation (11)] by the average growth rate of the grains within a topological class. This relationship is also time-invariant and independent simulation runs give nearly identical results.

Hillert [3] suggested the following relationship between the growth rate of an individual grain and its radius:

$$\frac{dR}{dt} = k \left(\frac{1}{R_{cr}} - \frac{1}{R} \right) \quad (12)$$

where R is the radius of the grain and k is a constant. R_{cr} is a critical radius such that grains with radii less than R_{cr} will shrink and those with radii larger than R_{cr} will grow. In two-dimensions, R_{cr} may be equal to the average grain radius $\langle R \rangle$. This equation was also derived in two dimensions by Lücke *et al.* [15] based on first principles and topological arguments. This equation is quantitatively tested by plotting dR/dt vs $(1/R - 1/\langle R \rangle)$ for individual grains, as in Fig. 11. An obvious feature of this plot is the large fluctuation of the data, especially for small size grains. The highest density of grains occurs at $1/R - 1/\langle R \rangle = 0$ where the size distribution function is maximal ($R/\langle R \rangle = 1$). There is no clear linear relationship in this plot. The average growth rates over 4000 grains at certain $(1/R - 1/\langle R \rangle)$ intervals are replotted in Fig. 12. In this figure, the dashed line is the data extracted by using interval $\Delta(1/R - 1/\langle R \rangle) = 0.01$ for the averaging and the solid dots interval $\Delta(1/R - 1/\langle R \rangle) = 0.05$. The solid line is the linear fit to the average data. It can be seen that the data near the average size region ($1/R - 1/\langle R \rangle = 0$) fit to the straight line quite well. As the grain size departs from the average size, the degree of data fluctuation increases. Especially when the grains become smaller

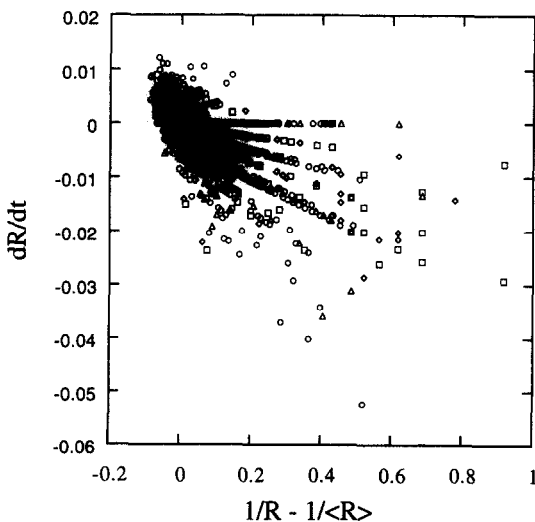


Fig. 11. Dependence of growth rate dR/dt on $1/R - 1/\langle R \rangle$ (Hillert equation) for individual grains. In this plot, more than 4000 grains were measured at different time steps and independent runs.

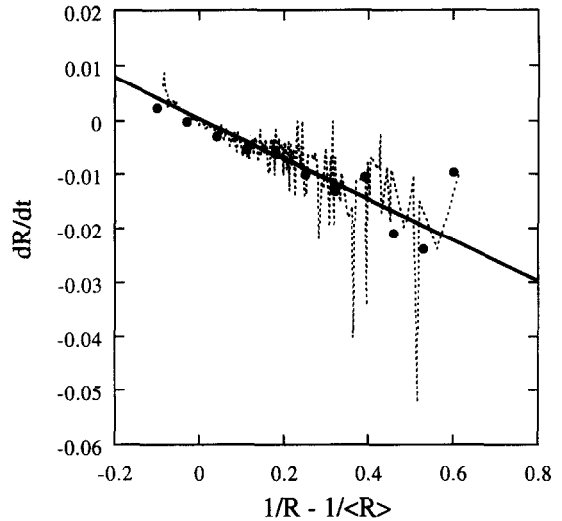


Fig. 12. Average data for dependence of growth rate dR/dt on $1/R - 1/\langle R \rangle$ (Hillert equation). The dashed line was averaged with the interval $\Delta(1/R - 1/\langle R \rangle) = 0.01$ and the solid dots were averaged with the interval $\Delta(1/R - 1/\langle R \rangle) = 0.05$. The solid line is the linear fit to the average data.

and smaller, the deviation of the growth rate from Hillert's equation becomes more and more severe. One of the reasons is that only very few small grains exist at a certain time step and hence the statistics are poor. However, it is clear that each individual grain may not follow Hillert's equation if the mean grain size is used as the critical size R_{cr} .

In the mean field theories, grain growth is viewed as a grain flux in the distribution space. Therefore, individual growth rates of grains in the distribution space may be used to study the behaviour of the grain evolution in distribution space. Following Srolovitz *et al.* [37], the growth rates dR/dt were normalized with $\langle R \rangle$ and $d(R/\langle R \rangle)/dt$ was plotted against $R/\langle R \rangle$ in the distribution space. The growth rates $d(R/\langle R \rangle)/dt$ for more than 4000 grains are shown in Fig. 13. Figure 14 is the average data with interval $\Delta(R/\langle R \rangle) = 0.01$. A large fluctuation of $d(R/\langle R \rangle)/dt$ for individual grains is observed. However, Fig. 14 shows that small grains ($R/\langle R \rangle$ less than 0.5) have a large negative $d(R/\langle R \rangle)/dt$, i.e. they rapidly shift to the small side of the distribution. For large grains ($R/\langle R \rangle$ larger than 1.0), the change rates $d(R/\langle R \rangle)/dt$ are much smaller and a small positive value is obtained on the average, which indicates that large grains move very slowly to the large side of the distribution. The above results essentially agree with the Monte Carlo simulations except that for grains with $R/\langle R \rangle$ larger than 1.0 a zero change rate was reported in the Monte Carlo simulation [37].

5. DISCUSSION

One interesting observation to be noticed in Fig. 2 is that the shapes of size distributions for each topological class may not be the same and it is not

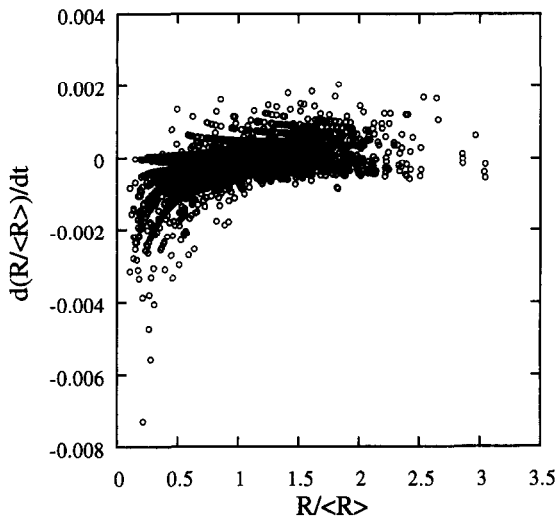


Fig. 13. Normalized growth rate $d(R/\langle R \rangle)/dt$ in normalized grain size ($R/\langle R \rangle$) space for individual grains. In this plot, more than 4000 grains were measured at different time steps and independent runs.

necessary to have the same distribution as the total distribution. The asymmetric feature of the total distribution function mainly comes from the 5-, 6- and 7-sided grains, which have highest probabilities of occurrence and dominate the shape of the total distribution. For few-sided and many-sided grains, the distributions are more symmetric than those of 5-, 6- and 7-sided grains. Even though the peak of the size distribution for 6-sided grains is highest among all the topological classes, the 5-sided grains have the highest probability of occurrence as shown in Fig. 3, the main reason being that 5-sided grains have a wider size distribution than 6-sided grains.

The present simulation (Figs 3 and 5) shows that the shape distribution is also time-invariant, indicat-

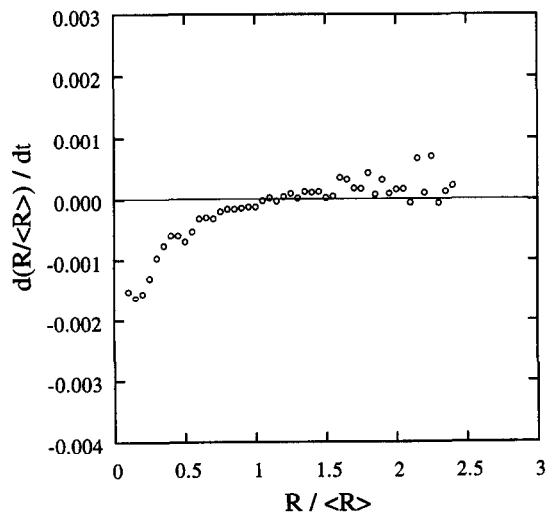


Fig. 14. Average data for normalized growth rate $d(R/\langle R \rangle)/dt$ in normalized grain size ($R/\langle R \rangle$) space. The data in Fig. 12 were averaged with interval $\Delta(R/\langle R \rangle) = 0.01$ in this figure.

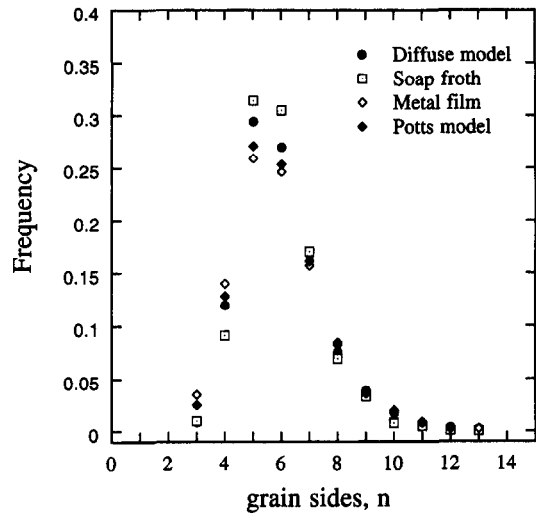


Fig. 15. Comparison of grain edge distributions between current study, Potts simulation, soap froth and experimental results in Al thin films [17, 37, 39].

ing that the “scaling” nature of normal grain growth applies both to the size distribution and to the shape distribution in two dimensions. This result seems to be consistent with the Potts model simulations and soap froth experiments [37, 39]. The shape distributions from the present simulation, the Potts model simulation [39], experimental observations of soap froth [39] and grain growth in Al thin films [17] are compared in Fig. 15. It can be seen that the shapes of these distributions from different sources are very similar and all of them have a maximum at 5-sided grains. However, simulations based on the mean field theory predicted a peak at 6-sided grains [17, 31]. The ratio of the frequency of occurrence of 5-sided grains to that of 6-sided grains, $\rho(5)/\rho(6)$, is 1.09 in the present simulation, 1.07 in the Potts model simulation, 1.05 in grain growth in metallic thin films and 1.03 in soap froth, which are identical within the statistical error. However, a careful examination of the distributions indicates that the shape distribution from soap froth has significantly lower values for many-sided grains than those in other distributions. The distribution data from different sources are tabulated in Table 1 for a more detailed comparison. One reason for this difference could be the fact that, intrinsically, many-sided grains are not favoured in soap froth experiments, and the fact that large and many-sided bubbles are more likely to touch the boundary in soap froth experiments and hence are excluded from the measurement and statistics analysis [39]. Another reason could be due to the coalescence which occurred in the present simulation as well as in Monte Carlo simulations as a result of the finite number of grain orientations, resulting in the formation of many-sided grains.

The second moment of the shape distribution, $\mu_2 = 2.33 \pm 0.13$, obtained in the present simulation, is close to that obtained in the Monte Carlo

Table 1. Data of grain edge distributions from simulations and experiments

Edges	Present model	Soap froth [39]	Metal film [17]	Potts model [39]
3	0.0088	0.0100	0.0350	0.0250
4	0.1192	0.0910	0.1400	0.1280
5	0.2936	0.3140	0.2590	0.2710
6	0.2694	0.3050	0.2460	0.2530
7	0.1666	0.1700	0.1570	0.1610
8	0.0752	0.0690	0.0820	0.0840
9	0.0385	0.0330	0.0360	0.0390
10	0.0175	0.0080	0.0200	0.0190
11	0.0053	0.0050	0.0090	0.0080
12	0.0038	0.0008	0.0020	0.0030
13	0.0020	0.0003	0.0025	

simulation (2.49) and to that measured in Al films (2.90). However, it is significantly higher than the soap froth result 1.5 ± 0.3 [39]. The difference in μ_2 between soap froth and Monte Carlo simulations as well as Al film results was originally believed to be the result of lattice anisotropy in the Potts model [39]. In the present continuum diffuse-interface model, however, the anisotropy due to the discretization of the continuum equations is extremely small if there are enough grid points to resolve the grain boundaries [23]. We checked our results by choosing parameters that produce grain boundaries four times thicker than those in the present simulation, and indeed we obtained almost identical values for the second moment. This indicates that some other factors other than the lattice anisotropy must contribute to the differences in the second moment obtained from different sources. We believe that the difference in moments is due to much lower frequencies of occurrence for many-sided grains in soap froth data than the present simulation and Potts simulations. Values for moments are sensitive to the tail of the distribution on the side of the many-sided grains. For example, one percent of 13-sided grains will contribute to μ_2 as much as 0.49 and the same amount of 12-sided grains will contribute 0.36. To show how the tail of many-sided grains may influence the second moment, let us cut the tails of distributions for $n > 10$ and recalculate the second moments for the distributions from different sources. It can be seen in Table 2 that, after recalculation, the μ_2 values for the diffuse-interface model, Potts model and metal film are significantly less and agree much better with that in the soap froth. It is noticed in Table 1 that for 6-sided grains soap froth data have the highest probability; the data from the present simulation have the second highest value, with the Potts model third, and metal film data the lowest (Fig. 15), whereas the μ_2 value increases in this order. Hence, the smaller the tail of the distribution for many-sided grains, the higher the probability of 6-sided grains, and the lower the second moment. It should be

pointed out that the lattice anisotropy may also influence the values of moments. For example, the difference in second moments between the present model and the Potts model could be due to lattice anisotropy, which is small compared to the difference between the present model and soap froth data.

Lewis’s law [equation (9)] is based on the mathematical requirement for the balance between the space filling and entropy, whereas polycrystal aggregates are regulated not only by the space filling but also by physical constraints [1, 4] such as the balance of surface tensions. Both experimental results [19] and Potts model simulations [37] as well as our present simulation (Fig. 7) demonstrated that grain growth in polycrystalline materials departs from the Lewis law. It is the physical constraints that result in the linear relationship between the mean radius and the topological class n , i.e. the Feltham law [equation (10)]. Indeed, the Feltham law is reproduced by the present simulation (Fig. 7), the Potts model simulations and experiments [19, 37]. The linear relationship is well approximated by the equation $\langle R_n \rangle / \langle R \rangle = 0.248(n - 2)$ in the present simulation, which is almost identical to that obtained in Potts model simulations. However, there are subtle differences between our data and soap froth data. In our simulation, both few-sided and many-sided grains have larger average areas than Lewis’s law predicted while in the soap froth data many-sided bubbles have smaller areas than Lewis’s law predicted [39]. Our data fit into the Feltham law very well for many-sided grains (Fig. 8) whereas soap froth data are lower than the linear prediction. This is another indication that there are fewer large many-sided grains in soap froth.

Another property which can be extracted from grain areas and topological classes is the so-called geometric factor α , which is the ratio of the kinetic coefficient k ($k = \alpha\pi M\sigma/3$) in the power growth law ($d_n^2 - d_0^2 = kt$) to the kinetic coefficient k_n ($k_n = \pi M\sigma/3$) in the Mullins–Von Neumann law [equation (11)].

Table 2. μ_2 values before and after cutting the tail of distribution

	Diffuse model	Soap froth	Metal film	Potts model
Before	2.31	1.81	2.68	2.47
After	1.66	1.51	1.94	1.86

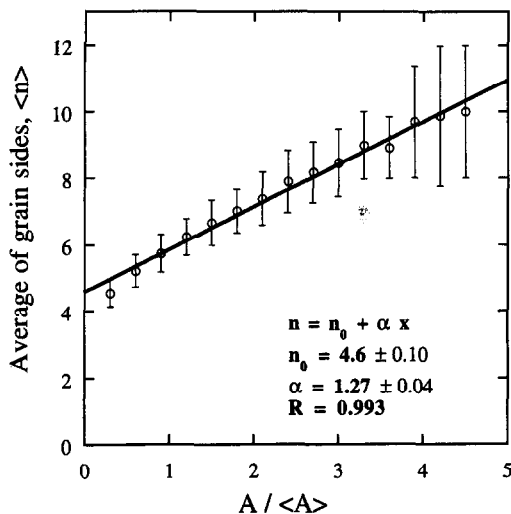


Fig. 16. Dependence of average grain edges $\langle n \rangle$ on normalized grain size $A/\langle A \rangle$. The individual data was averaged with interval $\Delta(A/\langle A \rangle) = 0.3$ in this plot. The solid line is the linear fit to the equation $\langle n \rangle = \langle n_0 \rangle + \alpha(A/\langle A \rangle)$, where α is the geometrical factor.

Fradkov [16] showed that the geometrical factor α can be expressed as

$$\alpha = \frac{d\langle n \rangle}{d(A/\langle A \rangle)} \quad (13)$$

where $\langle n \rangle$ is the average number of grain edges for all grains in a given area interval $A/\langle A \rangle$. Following Palmer *et al.* [20], the dependence of the average number of grain sides as a function of $A/\langle A \rangle$ is shown in Fig. 16 with interval $\Delta(A/\langle A \rangle) = 0.3$. The data were obtained by examining about 4000 grains. The slope of the linear fit gives $\alpha = 1.27 \pm 0.04$ which is almost identical to the experimental result 1.28 ± 0.05 obtained in succinonitrile (SCN) thin films [20].

It is widely accepted in theories and analyses that only 3-sided grains undergo vanishing in two-dimensional grain growth, and 4- and 5-sided grains have to transform to 3-sided ones through, neighbour switching before vanishing. A rather surprising result in Fig. 16 is that when the average area goes to zero, the average number of grain sides $n_0 = 4.59 \pm 0.04$. A very similar value has also been obtained from *in situ* observation of two-dimensional grain growth in SCN [22]. The value 4.59 for n_0 indicates that the majority of grains undergoing vanishing are 4- and 5-sided grains in 2 dimensions. Indeed, in our simulations, many grains stay in the 4-sided class before transforming to a disorder region where a junction of four grain boundaries is formed. All these simulation and experimental results prove that the vanishing of 4- and 5-sided grains is an important and common feature of 2-dimensional grain growth and should be included in theories which intend to describe 2-dimensional grain growth.

By time-differentiating Lewis's law [equation (9)], Rivier [10] gave a similar equation to the Mullins-Von Neumann law, i.e.

$$\frac{d\langle A_n \rangle}{dt} = C_7(n - 6) \quad (14)$$

where $\langle A_n \rangle$ is the average area of n -sided grains and C_7 is a constant. The data obtained from the present simulation are plotted in Fig. 17. Although the dependence of $d\langle A \rangle/dt$ on n appears to be linear, the n at which $d\langle A \rangle/dt$ is zero is about 4 instead of 6 as in equation (14). One of the reasons for this disagreement may be the fact that this equation comes purely from the mathematical requirement of space-filling, and surface tension constraints are not considered.

The conclusion that the Mullins-Von Neumann law [equation (11)] holds on average is consistent with recent experimental results in SCN thin films [20] and in soap froth [47-49]. Soap froth experiments [47, 48] showed that the average internal angles of bubbles were not exactly 120° , which is assumed in the derivation of equation (11). The deviation of the internal angles from 120° in soap froth is attributed to the presence of plateau borders in soap froth [49], and it is found that the Mullins-Von Neumann law is obeyed by individual bubbles in a drained froth with extremely narrow plateau borders [50]. Therefore, it is clear that the deviation of the growth rate from the Mullins-Von Neumann law for individual grains is due to the fact that the equilibrium assumed in equation (11) at vertices cannot be simultaneously achieved at each vertex during grain growth. It should be pointed out that, in soap froth, the diffusion process along boundaries is much faster than that across boundaries, which means that the equilibrium at vertices can be achieved quickly and the curvature of a bubble wall is constant in soap froth. On the other hand, in the grain growth of

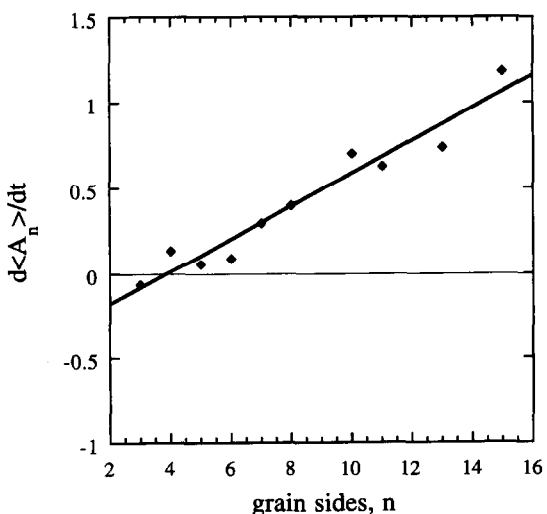


Fig. 17. Relationship between averaged growth rate $d\langle A_n \rangle/dt$ and the topological class n .

polycrystalline materials and in the current model, the time taken to reach equilibrium at vertices is much longer and the curvature of a grain varies from place to place. As a result, much wider deviations from equation (11) for each topological class are observed in the current simulations (Fig. 10) and in SCN thin films [20].

In equation (12), the driving force for grain growth is assumed to depend only on the grain size. Our simulation results (Fig. 12) indicate that this assumption may be valid near the mean grain size region if the mean grain size is used as the critical size R_{cr} . For large and small grains, deviations from this assumption are severe. We believe that the driving force for grain growth is dependent on both topological class and relative grain size, i.e. the behaviour of individual grains may be governed by a combination of, or competition between, the Von Neumann law or Hillert relationship. For example, many-sided grains tend to grow because they have concave boundaries and normally are larger than neighbour grains; however, the curvature and growth rate of each grain really depend on its size relative to those of neighbouring grains, and this is the reason for the fluctuation of growth rates (Figs 9–12). Similarly, few-sided grains tend to shrink due to convex curvature, but if a few-sided grain is relatively large it may not change its size within a certain time interval because the driving force is small. For 5-, 6- and 7-sided grains, their curvatures depend on their size and on neighbouring grains. If they are large and near small few-sided grains, they may have concave boundaries and grow; otherwise, they may shrink. These features can be clearly seen in Figs 9 and 10. However, there may not be a global critical radius R_{cr} which applies to each grain and it is really dependent on the individual grain and its neighbouring grains.

The dependence of the growth behaviour of an individual grain on the topological class, grain size and neighbouring grains results in randomness in the grain growth process. The randomness comes from the fact that the relationship between a grain and its neighbour grains cannot be predicted exactly even though the correlation exists between grains. In systems of isotropic grain boundary energies, grain growth is always driven by the curvature effects which are particularly dominant for small few-sided grains and large many-sided grains, while randomness may influence the growth rates and direction of 5-, 6- and 7-sided grains. The change rate $d(A/\langle A \rangle)/dt$ in the distribution space (Figs 13 and 14) may not give the evolution direction of a grain. For example, if the area of a grain does not change within a given time interval while the average area of all grains has increased, a negative change rate will be obtained in the distribution space. This negative rate means that this grain moves to a smaller size group because of the growth of other grains and it may not be the evidence of grain shrinkage. In this simulation, the shrinkage of large many-sided grains is not observed,

indicating the dominance of curvature effects during grain growth.

6. CONCLUSIONS

Based on the computer simulation results of grain growth in two dimensions using a diffuse-interface model, we arrive at the following conclusions:

(1) The shape distribution $\rho(n)$ is time-invariant and the peak is found at $n = 5$, consistent with experimental results and Potts model simulations, but different from the simulations based on the mean field theories which predicted a peak at $n = 6$.

(2) The second moment of the shape distribution $\mu_2 = 2.33$ is close to that obtained in Potts model simulations and metallic films. The departure of our data from that of soap froth is shown to be mainly a result of the difference in frequencies for many-sided grains in soap froth data and our simulations. The possible origins for the difference are discussed.

(3) The correlation between grains is observed and the Aboav–Weaire law is confirmed.

(4) Although our simulation results do not follow the Lewis law, the data fit to the Feltham law quite well.

(5) The Mullins–Von Neumann law is found to hold on average, whereas Hillert's relationship is obeyed near the mean grain size region if the mean grain size is used as the critical size R_{cr} . Based on the local kinetics for individual grains and the relationship with the topological class, the factors controlling the behaviour of individual grains are discussed.

(6) The randomness of growth rates for individual grains comes from the uncertainty of locally topological arrangements and the relative sizes of neighbouring grains.

Acknowledgements—This work is supported by the National Science Foundation under grant number DMR 93-11898 and the simulations were performed at the Pittsburgh Supercomputing Center.

REFERENCES

1. H. V. Atkinson, *Acta metall.* **36**, 469 (1988).
2. J. E. Burke and D. Turnbull, *Prog. Metal Phys.* **3**, 220 (1952).
3. M. Hillert, *Acta metall.* **13**, 227 (1965).
4. P. Feltham, *Acta metall.* **5**, 97 (1957).
5. N. P. Louat, *Acta metall.* **22**, 721 (1974).
6. D. Lewis, *Anat. Rec.* **38**, 351 (1928).
7. C. S. Pande, *Acta metall.* **36**, 2161 (1988).
8. F. N. Rhines and K. R. Craig, *Metal. Trans.* **5A**, 413 (1974).
9. I-Wei Chen, *Acta metall.* **35**, 1723 (1987).
10. N. Rivier, *Phil. Mag.* **B47**, L45 (1983).
11. J. von Neumann, *Metal Interfaces*, p. 108. ASM, Cleveland, OH (1952).
12. W. W. Mullins, *J. appl. Phys.* **27**, 900 (1956).
13. W. W. Mullins, *J. appl. Phys.* **59**, 1341 (1986).
14. G. Abbruzzese, I. Heckelmann and K. Lücke, *Acta metall.* **40**, 519 (1992).

15. K. Lücke, I. Heckelmann and G. Abbruzzese, *Acta metall.* **40**, 533 (1992).
16. V. E. Fradkov, *Phil. Mag. Lett.* **58**, 271 (1988).
17. V. E. Fradkov, L. S. Shvindlerman and D. G. Udler, *Scripta metall.* **19**, 1285 (1985).
18. C. V. J. Beenakker, *Phys. Rev. Lett.* **57**, 2454 (1986).
19. J. A. Glazier, S. P. Gross and J. Stavans, *Phys. Rev. A* **36**, 306 (1987).
20. M. Palmer, K. Rajan, M. Glicksman, V. Fradkov and J. Nordberg, *Metall. Mater. Trans. A* **26A**, 1061 (1995).
21. C. S. Smith, *Trans. Am. Soc. Metals* **45**, 533 (1953).
22. V. E. Fradkov, M. E. Glicksman and K. Rajan, in *Modeling of Coarsening and grain Growth* (edited by S. P. Marsh and C. S. Pande), p. 183. TMS, Warrendale, PA U.S.A. (1993).
23. Danan Fan and L.-Q. Chen, *Acta mater.* **45**, 611 (1997).
24. N. Rivier, *Phil. Mag.* **B52**, 795 (1985).
25. W. W. Mullins, *Scripta metall.* **22**, 1441 (1988).
26. R. M. C. de Almeida and J. R. Iglesias, *J. Phys. A* **21**, 3365 (1988).
27. R. L. Fullman, in *Metal Interfaces*, p. 179. American Society for Metals, Cleveland (1952).
28. K. Kawasaki, T. Nagai and K. Nakashima, *Phil. Mag. B* **60**, 399 (1989).
29. D. Weaire, F. Bolton, P. Molho and J. A. Glazier, *J. Phys.: Condens. Matter* **3**, 2101 (1991).
30. D. Weaire and H. Lei, *Phil. Mag. Lett.* **62**, 427 (1990).
31. C. W. J. Beenakker, *Phys. Rev. A* **37**, 1697 (1988).
32. M. Marder, *Phys. Rev. A* **36**, 438 (1987).
33. C. V. Thompson, H. J. Frost and F. Spaepen, *Acta metall.* **35**, 887 (1987).
34. S. Kumar, S. K. Kurtz, J. R. Banavar and M. G. Sharma, *J. Stat. Phys.* **67**, 523 (1992).
35. S. K. Kurtz and F. M. A. Carpay, *J. Appl. Phys.* **51**, 5125 (1980).
36. M. P. Anderson, D. J. Srolovitz, G. S. Grest and P. S. Sahni, *Acta metall.* **32**, 783 (1984).
37. D. J. Srolovitz, M. P. Anderson, P. S. Sahni and G. S. Grest, *Acta metall.* **32**, 793 (1984).
38. M. P. Anderson and G. S. Grest, *Phil. Mag. B* **59**, 293 (1989).
39. J. A. Glazier, *Phil. Mag. B* **62**, 615 (1990) and references therein.
40. L.-Q. Chen, *Scripta metall. Mater.* **32**, 115 (1995).
41. L.-Q. Chen and W. Yang, *Phys. Rev. B* **50**, 15 752 (1994).
42. L.-Q. Chen and D. Fan, *J. Am. Ceram. Soc.* **79**, 1163 (1996).
43. J. W. Cahn, *Acta metall.* **9**, 795 (1961).
44. J. W. Cahn and J. E. Hilliard, *J. Chem. Phys.* **28**, 258 (1958).
45. D. A. Aboav, *Metallography* **3**, 383 (1970).
46. D. Weaire, *Metallography* **7**, 157 (1974).
47. J. A. Glazier and J. Stavans, *Phys. Rev. A* **40**, 7398 (1989).
48. J. Stavans and J. A. Glazier, *Phys. Rev. Lett.* **62**, 1318 (1989).
49. D. Weaire and F. Bolton, *Phys. Rev. Lett.* **65**, 3449 (1990).
50. J. Stavans, *Phys. Rev. A* **42**, 5049 (1990).